Available online at www.sciencedirect.com
ScienceDirect
Journal of the European Ceramic Society 31 (2011) 1677–1683
www.elsevier.com/locate/jeurceramsoc

Lanthanum–titanium–aluminum oxide: A novel thermal barrier coating material for applications at 1300 °C

Xiaoyun Xie [a], Hongbo Guo [a,b,*], Shengkai Gong [a,b], Huibin Xu [a,b]

[a] School of Materials Science and Engineering, No. 37 Xueyuan Road, Beijing 100191, China
[b] Key Laboratory of Aerospace Materials & Performance (Ministry of Education), School of Materials Science and Engineering, No. 37 Xueyuan Road, Beijing 100191, China

Received 6 November 2010; received in revised form 13 March 2011; accepted 20 March 2011
Available online 12 April 2011

Abstract

Considerable efforts are being invested to explore new thermal barrier coating (TBC) materials with higher temperature capability to meet the demand of advanced turbine engines. In this work, $LaTi_2Al_9O_{19}$ (LTA) is proposed and investigated as a novel TBC material for application at 1300 °C. LTA showed excellent phase stability up to 1600 °C. The thermal conductivities for LTA coating are in a range of 1.0–1.3 $W\,m^{-1}\,K^{-1}$ (300–1500 °C) and the values of thermal expansion coefficients increase from 8.0 to $11.2 \times 10^{-6}\,K^{-1}$ (200–1400 °C), which are comparable to those of yttria stabilized zirconia (YSZ). The microhardness of LTA and YSZ coatings were in the similar level of ~7 GPa, however, the fracture toughness value was relatively lower than that of YSZ. The lower fracture toughness was compensated by the double-ceramic LTA/YSZ layer design, and the LTA/YSZ TBC exhibited desirable thermal cycling life of nearly 700 h at 1300 °C.

Keywords: Thermal barrier coatings; Thermal conductivity; Thermal expansion; Mechanical properties; Thermal shock resistance

1. Introduction

Thermal barrier coatings (TBCs) made of low-thermal conductivity ceramics have seen extensive applications in turbine engines used for aircraft propulsion, power plant, and marine propulsion to provide thermal insulation to metallic components from hot burner gas. Yttria stabilized zirconia (YSZ) is the current industrial standard topcoat materials in TBC system, which can long-term operate at temperatures below 1200 °C.[1–6] At higher temperatures, the phase transformation and accelerated sintering of YSZ tend to lead to early spallation failure of TBC.[7,8] To meet the development of advanced gas-turbine engines that operated at higher gas temperature, great efforts have been made to seek for new ceramic materials with better performance than YSZ.[9–11] The new materials cover especially doped zirconia,[12–14] pyrochlores,[15–17] perovskites,[18,19] and aluminates.[20–23]

Compared with YSZ, pyrochlore $La_2Zr_2O_7$ (LZ) has a lower thermal conductivity and better sintering-resistance. However, the LZ coating has a very short life due to its low thermal expansion coefficient (TEC) compared to YSZ, which leads to higher thermal stresses from thermal expansion mismatch.[15] CeO_2 was considered to substitute for ZrO_2 because materials containing CeO_2 usually have higher TECs and lower thermal conductivity than YSZ. $La_2Ce_2O_7$ (LC) is a solid solution of La_2O_3 in CeO_2 with a defect fluorite structure. The main advantages of LC as TBC material are low thermal conductivity and no phase transformation between room temperature and 1400 °C.[24] But the thermal expansion shows a sudden decrease in the temperature range of 200–400 °C and LC reacts with α-Al_2O_3 at high temperature, resulting in poor thermal cycling life of the single layer LC TBC.[24,25] It seems that the double-layered topcoat design can overcome the shortcomings and improve the thermal cycling lives of LZ and LC coatings.[26–28] Recently, a large class of hexaluminates with magnetoplumbite structure, particularly the $LaMgAl_{11}O_{19}$ (LMA), have been proposed as new TBC materials for the excellent sintering-resistance.[20–23] The LMA prevents sintering and thus exhibits improved ageing behavior under long-term thermal loads despite its relative higher thermal conductivity than that of YSZ TBC.[22] Lanthanum

* Corresponding author at: School of Materials Science and Engineering, No. 37 Xueyuan Road, Beijing 100191, China. Tel.: +86 10 8231 7117; fax: +86 10 8233 8200.
E-mail address: Guo.hongbo@buaa.edu.cn (H. Guo).

0955-2219/$ – see front matter © 2011 Elsevier Ltd. All rights reserved.
doi:10.1016/j.jeurceramsoc.2011.03.036

Table 1
Nominal chemical composition of Ni-based superalloy K3 (in wt.%).

Ni	Co	Cr	Al	Ti	Mo	W	Fe
Bal.	4.5–6.0	10.0–12.0	5.3–5.9	2.3–2.9	3.8–4.5	4.8–5.5	<2.0

titanium aluminum oxide ($LaTi_2Al_9O_{19}$, LTA) is face-centered monoclinic with a huge unit cell, which is as four times large as that of the magnetoplumbite phase and interleaved with pseudobrookite-like layers. The special crystallographic sites could allow achieving the capability of a lower thermal conductivity. In this work, $LaTi_2Al_9O_{19}$ was proposed as a novel TBC material. The phase stability, thermophysical properties and mechanical properties of the LTA were investigated. Besides, the durability of the plasma-sprayed coating was evaluated by thermal cycling testing at 1300 °C.

2. Experimental procedure

LTA materials were synthesized by solid-state reaction of La_2O_3 (99.99%), TiO_2 (≥99.7%) and Al_2O_3 (≥99.7%). The three powders were ball-milled directly, after drying, calcined at 1500 °C for 24 h. This process was repeated for three times to obtain pure products. The LTA compact was densified by cold pressing of LTA powders at 400 MPa, followed by sintering at 1600 °C for 72 h.

The powders for plasma-spraying were produced by the spraying method and the powders of 25–150 μm were selected for spraying. Ni–21Co–17Cr–12Al–1Y (in wt.%) bond coat was sprayed onto disk shaped K3 Ni-based superalloy substrate (Φ 30 mm × 2.5 mm) by vacuum plasma spraying with an F4 gun. The chemical composition of the K3 superalloy is listed in Table 1. Then the LTA coating was deposited on the bond coat in an atmospheric plasma spraying unit using a 7-M gun (Sulzer Metco). For manufacturing of the LTA/YSZ double-ceramic-layered TBC, the YSZ coating was sprayed from 204 NS feedstocks (Sulzer Metco) as the bottom ceramic layer while the LTA coating was deposited as the top ceramic layer. The processing parameters used for spraying LTA and YSZ are given in Table 2. The sprayed coatings were annealed in air at 1050 °C for re-crystallization. Free-standing LTA coatings, which were used to investigate the thermophysical properties and microstructure evolutions, were produced by spraying LTA powders onto the steel, followed by removing the substrate using chemical etching.

The crystal structure was characterized by XRD (X' Pert Pro MPD, Cu K*a* radiation, Netherlands). Phase stability and specific heat of the LTA specimen were investigated by differential scanning calorimeter (DSC, Netzsch STA 449C, Germany) in argon atmosphere with a heating rate of 20 °C min^{-1}. The density was determined by the principle of Archimedes' and the chemical composition of LTA coating was analyzed by electron probe micro-analysis (EPMA, JXA-8100, JEOL). The porosity of the coating was determined using mercury porosimeter (AUTOSCAN-33, QUANTA CHROME, USA). The coating microstructures were characterized on scanning electron microscopy (SEM, FEI Quanta 600, Netherlands).

Table 2
Processing parameters for plasma spraying of LTA and YSZ coating.

Powder	Power (kW)	Spray distance (mm)	Ar (slpm)	H_2 (slpm)	Feed rate (g min^{-1})
LTA	37.3	120	45	12	40
YSZ	38	75	38	17	35

Thermal diffusivity measurement was conducted in argon by laser flash diffusivity apparatus (Netzsch LFA 427, Germany) on the bulk and free-standing coating specimens with a diameter of 12.7 mm and thickness of 1–2 mm. Thermal expansion of LTA was determined using a high-temperature dilatometer (Netzsch DIL 402E, Germany) on the LTA bulk specimen with dimensions of 25 mm × 4 mm × 4 mm.

The micro-hardness was measured by micro-hardness indenter (HXZ-1000). Elastic modulus (*E*) was determined using the following equation:[29]

$$\frac{b'}{a'} = \frac{b}{a} - \frac{\alpha H_k}{E} \tag{1}$$

where b'/a' denotes the indent diagonal after elastic recovery during indentation; b/a is the ratio of the known Knoop indenter dimensions or geometry (1/7.11); α is a constant, having a value of 0.45; H is the Knoop microhardness value obtained from the indentation, while E is the Young's modulus. Test load of 2.94 N with a holding time of 15 s was used in this investigation. The fracture toughness was calculated based on the following equation:[30]

$$K_{IC} = 0.016\left(\frac{E}{H}\right)^{1/2}\left(\frac{P}{c^{3/2}}\right) \tag{2}$$

where K_{IC} denotes the fracture toughness (MPa m$^{1/2}$); H the hardness (GPa); E the elastic modulus obtained from Eq. (1) (GPa); P the indenter load (kgf) and c the crack length (μm).

The thermal cycling testing of LTA/YSZ TBCs was performed in a gas burner test facility operating with propane and oxygen. The coatings were heated for 20 s to the desired surface temperature and held for 10 min. During heating stage the backside of the sample was cooled by compressed air to maintain a controlled temperature gradient through the sample thickness. The surface temperature and the substrate temperature were measured with a pyrometer (Raytek, Model: MR1SBSF, USA, 0.75–1.1 μm, 0.95–1.1 μm) and a NiCr/NiSi thermocouple, respectively. During cooling stage the burner went out automatically to save the fuel and the sample was cooled by compressed air from both sides for 40 s to room temperature. Thermal cycling was stopped when visible spallation of the coating occurred. The lifetime of the TBCs is defined as the number of the cycles before failure of the coatings. Three samples were tested to obtain the average cyclic lifetime.

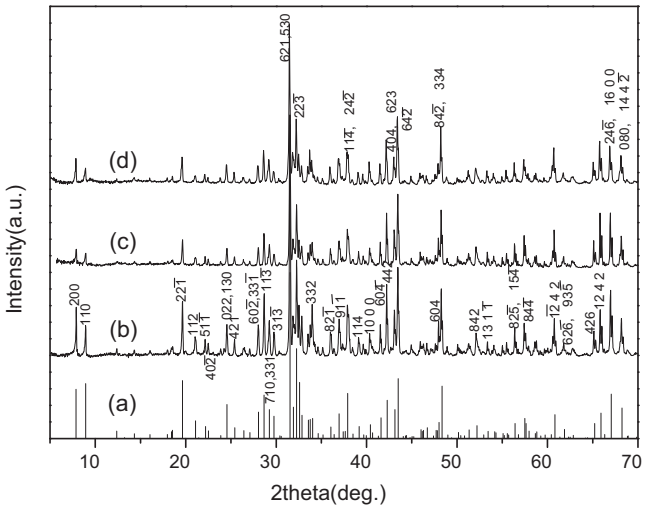

Fig. 1. XRD patterns of LTA: (a) JCPDS card No. 37-1233; (b) LTA powders; (c) LTA powders annealed at 1500 °C for 110 h; (d) LTA compact annealed at 1600 °C for 72 h.

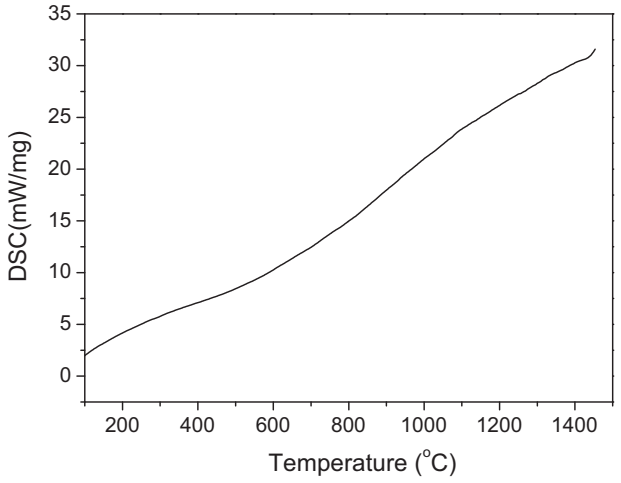

Fig. 2. DSC curve of LTA powders after annealing at 1500 °C for 110 h.

3. Results and discussion

3.1. Synthesis, phase stability and coating preparation

The X-ray diffraction (XRD) pattern of the synthesized LTA powder is shown in Fig. 1 (pattern b). Compared with the JCPDS card (pattern a), single LTA phase was obtained by solid-state reaction conducted at 1500 °C. According to the XRD result, the lattice parameters of LTA are calculated to be $a = 22.58$ Å, $b = 10.99$ Å, $c = 9.72$ Å and $\beta = 98.6°$, respectively, which agree well with JCPDS card. The major diffraction peaks are also indexed in Fig. 1, indicating the low symmetry and complex atoms arrangement within the unit cell. The crystallographic density was determined to be 4.35 g cm^{-3}, nearly 30% lower than that of YSZ (6.0 g cm^{-3}).

Fig. 1 also compares XRD patterns of LTA powders after 110 h heat-treatment at 1500 °C (pattern c) and LTA bulk densified by cold pressing of LTA powders and followed by sintering at 1600 °C for 72 h (pattern d). Decomposition and phase destabilization of the specimen did not occur during sintering and heat-treatment process, implying excellent high temperature capability of the LTA phase.

Phase stability of the LTA powder annealed at 1500 °C for 110 h was examined by differential scanning calorimeter (DSC). There are neither endothermic nor exothermic peaks from room temperature to 1450 °C in the DSC curve, as shown in Fig. 2. This indicates that phase transformation of LTA did not occur during heating and the LTA phase was stable at least up to 1450 °C.

The XRD patterns of the LTA coating as-sprayed and after 20 h heat-treatment at 1050 °C are presented in Fig. 3. The as-sprayed coating mainly comprised amorphous phase due to rapid heating and cooling during plasma spraying deposition (pattern a). If the coating is thermally cycled in an amorphous state, then the re-crystallization together with oxidation and thermal mismatch stresses could accelerate premature spallation failure of TBC. In this context, annealing of the sprayed coating was performed at 1050 °C for re-crystallization. After 20 h annealing, crystallization of the coating was completed (pattern b). Compared to the diffraction patterns of LTA powder, the annealed coating does not show any other peaks, suggesting that no decomposition occurred during plasma spraying. The chemical composition analysis of LTA coating shows atom ratio of La:Ti:Al ≈ 1:2:9, indicating that the LTA coating with stoichiometric composition was attained by plasma spraying.

The cumulative porosity distribution of the free-standing LTA coating is shown in Fig. 4. The result reveals a typical bimodal pore size distribution. According to Guo et al.,[31,32] the larger defects corresponding to radius above 1 μm are believed to have resulted from macrocracks and voids (globular and irregular pores). The fine pores with a size smaller than 1 μm are mainly attributed to microcracks such as intersplat gaps and intrasplat cracks. The cumulative porosity of the LTA coating is ~8%, which is relative lower than the optimized porosity level (12–15%) of traditional YSZ TBCs. The thermal insulation is dependent not only on the total porosity but also on the aspect

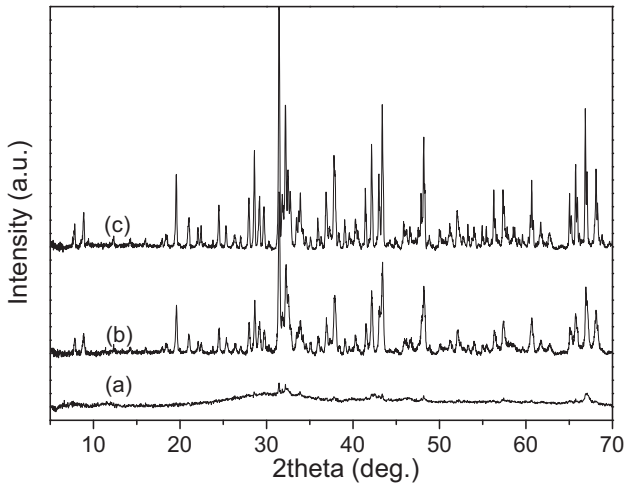

Fig. 3. XRD patterns of LTA coatings: (a) as-sprayed; (b) annealed at 1050 °C for 20 h; (c) after thermal cycling (equal to a holding time of nearly 700 h at 1300 ± 50 °C).

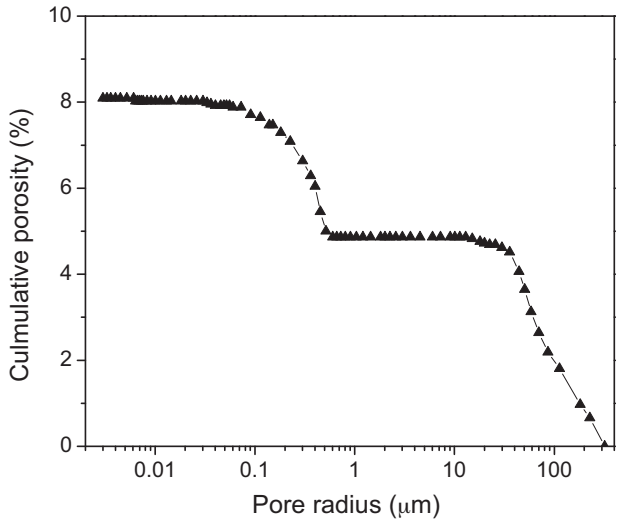

Fig. 4. Porosities distribution of as-sprayed LTA coating.

ratio of pores. The percentage of large pores as high as 60% suggests that the LTA coating should be further optimized with respect to the microstructure.

3.2. Thermophysical and mechanical properties

Thermophysical properties such as thermal diffusivity and thermal conductivity are important parameters for TBCs' thermal insulation. In electric isolating solids, the thermal resistivity is due to changes of lattice vibrations which are usually described as phonon scattering. After sintering at 1600 °C for 72 h, the density of the cold-pressed LTA bulk was determined to be 4.1 g cm^{-3} and the relative density reached 95%. The thermal diffusivity of the LTA bulk decreased from 1.2 mm^2 s^{-1} to 0.5 mm^2 s^{-1} when heating from 25 °C to 1400 °C, as shown in Fig. 5a. For the coating specimen with porosity around 8%, the lowest value of 0.3 mm^2 s^{-1} was achieved at 900 °C above which the thermal diffusivity revealed a little increase. The increased diffusivity could be attributed to re-crystallization of amorphous phase at high temperature. The specific heat capacity of the LTA specimen was measured by a differential scanning calorimeter from room temperature to 1400 °C and the values were coincidence with the calculated ones by the Neumann–Kopp rule, as shown in Fig. 5b.

Thermal conductivity was calculated according to the following equation:

$$\lambda = \kappa \rho C_p$$

where λ is the thermal conductivity, κ the thermal diffusivity, ρ the bulk density and C_p the specific heat. For comparison, the values of YSZ and some candidate materials being investigated are also presented in Fig. 5c with relative densities and porosity labeled in parentheses. Between 300 °C and 1500 °C, the thermal conductivities for the LTA coating are in a range of 1.0–1.3 W m^{-1} K^{-1}, which are comparable with 8YSZ TBC and much lower than those of LMA (2 W m^{-1} K^{-1}, 1200 °C). The low thermal conductivity of LTA is relevant to the complicated

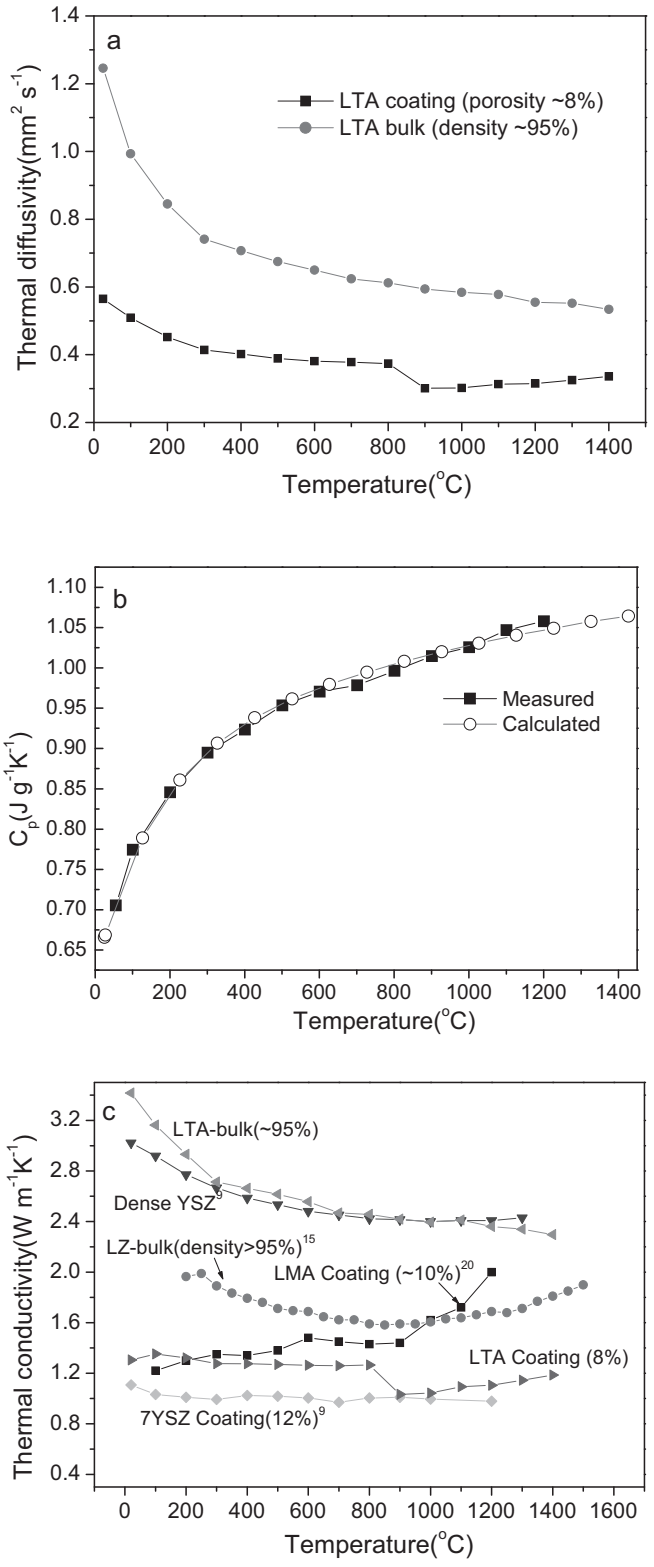

Fig. 5. (a) Thermal diffusivities of the LTA bulk (prepared by cold pressing and sintering at 1600 °C for 72 h) and sprayed coating (as coated), (b) specific heat capacities of LTA and (c) thermal conductivities for several candidate TBC materials (all the coatings mentioned here are as coated and produced by plasma spraying).

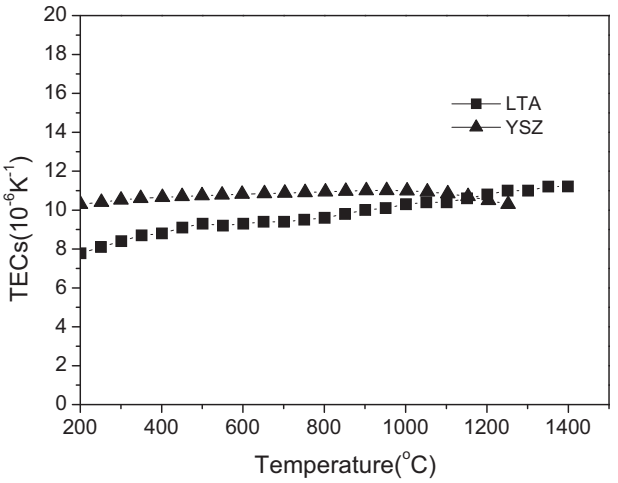

Fig. 6. Thermal expansion coefficients of LTA bulk specimen.

crystal structure which has a low symmetry and incorporates several crystallographic different atoms inside the unit cell. The huge unit cell and complex atoms arrangement result in the increase of scattering center and decrease of the mean free path of phonons with a consequent reduction of thermal diffusivity. Due to these, the LTA coating exhibits very promising thermal insulating performance for application as a TBC.

The thermal-expansion mismatch is one of the crucial factors responsible for spallation failure of TBCs. Large TECs are desirable for the ceramic topcoat in TBC systems because the large TECs tend to reduce thermal stresses arising from thermal expansion mismatch between the ceramic topcoat and metallic substrate and extend the thermal cycling life of the TBC. The TECs of LTA bulk are shown in Fig. 6. The LTA specimen expanded almost linearly in the temperature range of room temperature to 1400 °C and the values of TECs increased from 8.0×10^{-6} K^{-1} to 11.2×10^{-6} K^{-1} (200–1400 °C), which were very closed to the values of YSZ. At this point, the LTA is eligible for the topcoat materials in TBC system.

Besides the thermal properties, mechanical properties of ceramics are also very important for superior TBCs. The hardness values as well as Young's modulus and fracture toughness values for LTA and YSZ are given in Table 3. The microhardness for the LTA bulk is comparable to that of the YSZ bulk. Also, the microhardness for the LTA and YSZ coatings are in the similar level of ~7 GPa. The high microhardness enables TBC resist to erosion and foreign-object impact. The Young's modulus of the LTA bulk is 230–250 GPa, a little higher than that of the YSZ bulk. The Young's moduli for both of the coatings are 85–115 GPa. The values for the Young's modulus of the YSZ coating reported in literatures are in a broad range of 50–100 GPa,[2,34,35] possibly owing to the variable and anisotropic microstructure of the plasma sprayed coatings. In addition, the measurement techniques may also affect the results. The fracture toughness was determined by an indentation technique. The values of 1.9–2.5 MPa m$^{1/2}$ for the LTA bulk are relatively lower than the values for the YSZ bulk (6–9 MPa m$^{1/2}$).[33] The values of 0.9–1.7 MPa m$^{1/2}$ for the LTA coating are nearly half of those for the YSZ coating. Lower

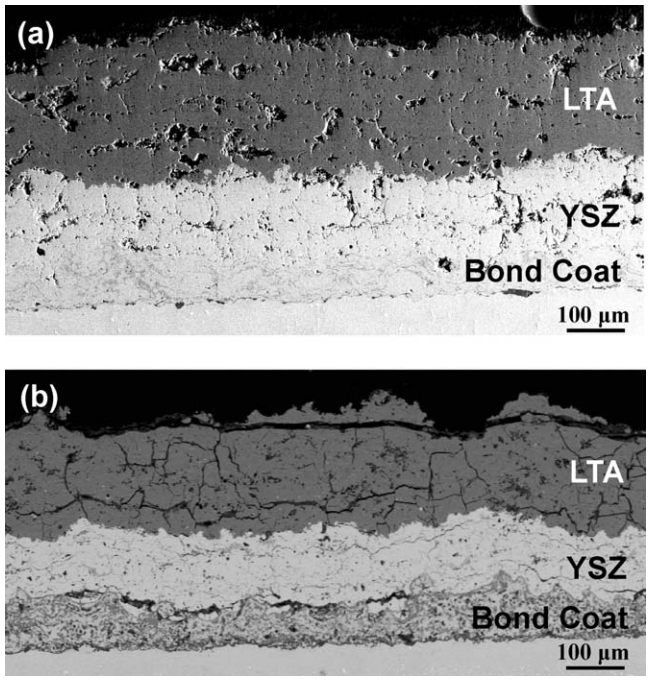

Fig. 7. SEM micrographs of cross-sections of the LTA/YSZ TBCs: (a) as-sprayed and (b) after thermal cycling.

fracture toughness is not desirable for TBCs because TBCs tend to be cracking more easily when suffering from large stresses. On the other hand, LTA kept chemical stable with ZrO_2 even at 1500 °C investigated by calcining the mixtures of powders of 50 mol% LTA and 50 mol% ZrO_2. In this context, LTA/YSZ double-ceramic-layered TBC was proposed, exhibiting a significant improvement in thermal cycling lifetime as compared to the single LTA TBC.

3.3. Thermal cycling performance of LTA/YSZ TBCs

The cross-section micrograph of the plasma-sprayed LTA/YSZ TBC is shown in Fig. 7a. A NiCoCrAlY bond coat of ~100 μm thickness was coated onto the K3 substrate. An YSZ layer of ~200 μm thickness and a LTA layer with the nearly same thickness were sprayed onto the bond coat as the bottom ceramic layer and the upper ceramic layer, respectively. The binding of LTA layer to YSZ layer looks perfect, showing a good melting condition of LTA powder in the plasma flame. The LTA/YSZ TBC specimen was exposed to a gas flame for 10 min, followed by compressed air cooling for 40 s. For comparison, the LTA single-layered TBC was also evaluated. During heating process, the coating surface temperature was 1300 ± 50 °C, and the substrate temperature was 950 ± 50 °C. The average cyclic life of the LTA/YSZ TBC was 4189 cycles, which equalled to a holding time of nearly 700 h at 1300 ± 50 °C, whereas the LTA single-layered TBC had a short life of less than 800 cycles. Spallation failure of the single LTA TBC occurred at the interface between the ceramic top-coat and the bond coat, exhibiting the same failure mode with the traditional YSZ TBC. The peeling off may be owing to the thermal expansion mismatch between the LTA layer and bond coat (~14×10^{-6} K^{-1}) and the relative low

Table 3
Mechanical properties of LTA samples determined by indentation technique.

Sample	Hardness [GPa]	Young's modulus [GPa]	Fracture Toughness [MPa $m^{1/2}$]
YSZ-bulk (full dense)	13 ± 1[15]	210 ± 10[15]	6–9[33]
YSZ-coating (porosity: ~12%)	7.1 ± 0.2[a] 6.3[34]	93.1 ± 10.8[a] 50–100[2,34,35]	1.6–3.6[a] 1–3[15,36,37]
LTA-bulk (density: ~95%)	14.6 ± 1.2	240 ± 13	1.9–2.5
LTA-coating (porosity: ~8%)	7.1 ± 1.1	99.6 ± 13.4	0.9–1.7

[a] Determined in this work.

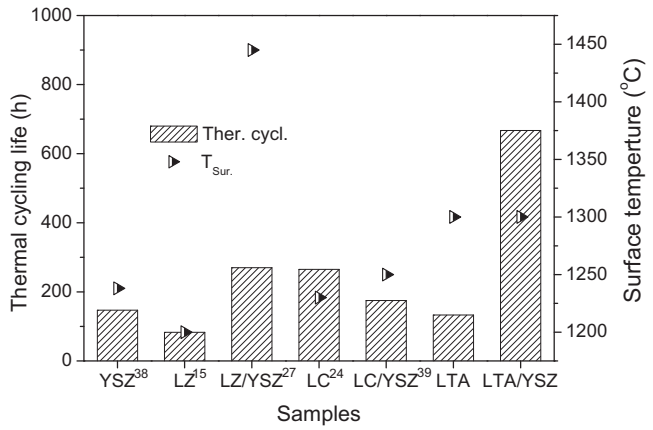

Fig. 8. Thermal cycling lives of LTA TBC and LTA/YSZ TBC as well as other TBC candidates for burner-rig test. See refs. [38,39].

fracture toughness of LTA. For the LTA/YSZ TBC, the upper LTA layer spalling bit by bit instead of peeling off in one piece was observed after around 4000 thermal cycles. Compared to the sprayed coating, there are a large number of cracks in the LTA layer after thermal cycling, as shown in Fig. 7b. The large irregular cracks, caused by the sintering of ceramic topcoat exposed to high temperature for long term, would result in the spalling of the coating surface under the erosion of high temperature and high-speed gas flame. According to the XRD pattern as shown in Fig. 3 (pattern c), the coating still remained the LTA phase even after 4000 thermal cycles, indicating a good phase stability. For comparison, the thermal cycling lives of the traditional YSZ TBC and some new TBCs reported in literatures are also presented in Fig. 8. All of the coatings were prepared by atmospheric plasma spraying and the thermal cycling lives of the coatings were assessed by gas-burner test facility. Despite of the varieties in coating microstructures and failure criterions, the LTA/YSZ TBC showed very promising thermal cycling performance at 1300 °C. It is expected that the thermal cycling life of the LTA/YSZ coating can be improved by further optimization of the process parameters and coating microstructure.

4. Conclusions

In conclusion, we investigated the synthesis, phase stability, thermophysical and mechanical properties, and thermal cycling performance of $LaTi_2Al_9O_{19}$ (LTA) TBC. As a new TBC material, LTA showed excellent phase stability between room temperature and 1600 °C. The thermal conductivities for the LTA coating are in a range of 1.0–1.3 $W\,m^{-1}\,K^{-1}$ (300–1500 °C) and the values of thermal expansion coefficients increase from $8.0 \times 10^{-6}\,K^{-1}$ to $11.2 \times 10^{-6}\,K^{-1}$ (200–1400 °C), which are comparable to those of yttria stabilized zirconia (YSZ). The microhardness of the LTA and YSZ coatings were in the similar level of ~7 GPa. However, the fracture toughness of LTA coating ranged from 0.9 to 1.7 MPa $m^{1/2}$, which were relative lower than that of YSZ. The lower fracture toughness was compensated by the double-ceramic LTA/YSZ layer design, and the LTA/YSZ TBC exhibited desirable thermal cycling life of nearly 700 h at 1300 °C. Due to the merits above, LTA is very promising candidate for TBC applications at temperatures at 1300 °C.

Acknowledgements

The research is sponsored by National Natural Science Foundation of China (NSFC, No. 50771009, No. 50731001 and No. 51071013) and National Basic Research Program (973 Program) of China under Grant No. 2010CB631200.

References

1. Miller RA. Current status of thermal barrier coatings—an overview. *Surf Coat Technol* 1987;**30**:1–11.
2. Padture NP, Gell M, Jordan EH. Thermal barrier coatings for gas-turbine engine applications. *Science* 2002;**296**(4):280–4.
3. DeMasi-Marcin JT, Gupta DK. Protective coatings in the gas turbine engine. *Surf Coat Technol* 1994;**68–69**:1–9.
4. Cernuschi F, Bianchi P, Leoni M, Scardi P. Thermal diffusivity/microstructure relationship in Y-PSZ thermal barrier coatings. *J Therm Spray Technol* 1999;**8**(1):102–9.
5. Xu HB, Gong SK, Zhang Y, Zhang CX. Experimental and computational study on hot fatigue process of thermal barrier coatings by EB-PVD. *Intermetallics* 2005;**13**(1–2):315–22.
6. Guo HB, Gong SK, Khor KA, Xu HB. Effect of thermal exposure on the microstructure and properties of EB-PVD gradient thermal barrier coatings. *Surf Coat Technol* 2003;**168**:23–9.
7. Miller RA, Smialek JL, Garlick RG. Phase stability in plasma-sprayed partially stabilized zirconia–yttria. In: Heuer AH, Hobbs LW, editors. *Advances in ceramics. Science and technology of zirconia*, vol. 3. Columbus, OH: American Ceramic Society; 1981. p. 241–51.
8. Zhu D, Miller RA. Sintering and creep behavior of plasma-sprayed zirconia- and hafnia-based thermal barrier coatings. *Surf Coat Technol* 1998;**108–109**:114–20.
9. Clarke DR, Phillpot SR. Thermal barrier coating materials. *Mater Today* 2005;**8**(6):22–9.
10. Cao XQ, Vaβen R, Stöver D. Ceramic materials for thermal barrier coatings. *J Eur Ceram Soc* 2004;**24**(1):1–10.
11. Vaβen R, JarligoMO, SeinkeT, Mack DE, Stöver D. Overviewon advanced thermal barrier coatings. *Surf Coat Technol* 2010;**205**(4):938–42.
12. Matsumoto M, Yamaguchi N, Matsubara H. Low thermal conductivity and high temperature stability of ZrO_2–Y_2O_3–La_2O_3 coatings produced by electron beam PVD. *Scripta Mater* 2004;**50**:867–71.
13. Rahaman MN, Gross JR, Dutton RE, Wang H. Phase stability, sintering and thermal conductivity of plasma-sprayed ZrO_2–Gd_2O_3 composi-

tions for potential thermal barrier coating applications. *Acta Mater* 2006;**54**:1615–21.
14. Wei QL, Guo HB, Gong SK, Xu HB. Novel microstructure of EB-PVD double ceramic layered thermal barrier coatings. *Thin Solid Films* 2008;**516**:5736–9.
15. Vaβen R, Cao X, Tietz F, Basu D, Stöver D. Zirconates as new materials for thermal barrier coatings. *J Am Ceram Soc* 2000;**83**:2023–8.
16. Lehmann H, Pitzer D, Pracht G, Vaβen R, Stöver D. Thermal conductivity and thermal expansion coefficients of the lanthanum rare-earth-element zirconate system. *J Am Ceram Soc* 2003;**86**:1338–44.
17. Yu JH, Zhao HY, Tao SY, Zhou XM, Ding CX. Thermal conductivity of plasma sprayed $Sm_2Zr_2O_7$ coatings. *J Eur Ceram Soc* 2010;**30**:700–804.
18. Ma W, Mack D, Malzbender J, Vaβen R, Stöver D. Yb_2O_3 and Gd_2O_3 doped strontium zirconate for thermal barrier coatings. *J Eur Ceram Soc* 2008;**28**:3071–81.
19. Guo HB, Zhang HJ, Ma GH, Gong SK. Thermo-physical and thermal cycling properties of plasma-sprayed $BaLa_2Ti_3O_{10}$ coating as potential thermal barrier materials. *Surf Coat Technol* 2009;**204**:691–6.
20. Friedrich C, Gadow R, Schirmer T. Lanthanum hexaluminate—a new material for atmospheric plasma spraying of advanced thermal barrier coatings. *J Therm Spray Technol* 2001;**10**:592–8.
21. Bansal NP, Zhu DM. Thermal properties of oxides with magnetoplumbite structure for advanced thermal barrier coatings. *Surf Coat Technol* 2008;**202**(12):2698–703.
22. Cao XQ, Zhang YF, Zhang JF, Zhong XH, Wang Y, Ma HM, et al. Failure of the plasma-sprayed coating of lanthanum hexaluminate. *J Eur Ceram Soc* 2008;**28**:1979–86.
23. Chen XL, Zhang YF, Zhong XH, Zhang JF, Cheng YL, Zhao Y, et al. Thermal cycling behaviors of the plasma sprayed thermal barrier coatings of hexaluminates with magnetoplumbite structure. *J Eur Ceram Soc* 2010;**30**:1649–57.
24. Cao XQ, Vaβen R, Fischer W, Tietz F, Jungen W, Stöver D. Lanthanum–cerium oxide as a thermal barrier-coating material for high-temperature applications. *Adv Mater* 2003;**17**:1438–42.
25. Ma W, Gong SK, Xu HB, Cao XQ. On improving the phase stability and thermal expansion coefficients of lanthanum cerium oxide solid solutions. *Scripta Mater* 2006;**54**:1505–8.
26. Cao X, Vaβen R, Tietz F, Stöver D. New double-ceramic-layer thermal barrier coatings based on zirconia–rare earth composite oxides. *J Eur Ceram Soc* 2006;**26**:247–51.
27. Vaβen R, Stöver D. New thermal barrier coatings based on pyrochlore/YSZ double layer systems. *Int J Appl Ceram Technol* 2005;**1**:351–61.
28. Ma W, Gong SK, Li HF, Xu HB. Novel thermal barrier coatings based on $La_2Ce_2O_7$/8YSZ double-ceramic-layer systems deposited by electron beam physical vapor deposition. *Surf Coat Technol* 2008;**202**:2704–8.
29. Marshall DB, Noma T, Evans GA. A simple method for determining elastic–modulus–hardness ratios using Knoop indentation measurements. *J Am Ceram Soc* 1982;**65C**:175–6.
30. Anstis GR, Chantikul P, Lawn BR, Marshall DB. A critical evaluation of indentation techniques for measuring fracture toughness. 1. Direct crack measurements. *J Am Ceram Soc* 1981;**64**:533–8.
31. Guo HB, Murakami H, Kuroda S. Effect of hollow spherical powder distribution on porosity and segmentation cracks in thermal barrier coatings. *J Am Ceram Soc* 2006;**89**:3797–804.
32. Guo HB, Kuroda S, Murakami H. Microstructures and properties of plasma-sprayed segmented thermal barrier coatings. *J Am Ceram Soc* 2006;**89**:1432–9.
33. Gupta TK. In: Bradt RC, Hasselman DPH, Lange FF, editors. *Fracture mechanics of ceramics*, vol. 4. New York/London: Plenum Press; 1978.
34. Choi SR, Zhu D, Miller RA. Effect of sintering on mechanical properties of plasma-sprayed zirconia-based thermal barrier coatings. *J Am Ceram Soc* 2005;**88**:2859–67.
35. Guo HB, Murakami H, Kuroda S. Effects of heat treatment on microstructures and physical properties of segmented thermal barrier coatings. *Mater Trans* 2005;**46**:1775–8.
36. Taylor R, Brandon JR, Morrell P. Microstructure, composition and property relationship of plasma-sprayed thermal barrier coatings. *Surf Coat Technol* 1992;**50**:141–9.
37. Beshish GK, Florey CW, Worzala FJ, Lenling WJ. Fracture toughness of thermal spray ceramic coatings determined by the indentation technique. *J Therm Spray Technol* 1993;**2**:35–8.
38. Guo HB, Vaβen R, Stöver D. Atmospheric plasma sprayed thick thermal barrier coatings with high segmentation crack density. *Surf Coat Technol* 2004;**186**:353–63.
39. Guo HB, Wang Y, Wang L, Gong SK. Thermo-physical properties and thermal shock resistance of segmented $La_2C_2O_7$/YSZ thermal barrier coatings. *J Therm Spray Technol* 2009;**18**:665–71.